Chemistry Europe
European Chemical Societies Publishing

WILEY VCH

Excellence in Chemistry Research

Announcing our new flagship journal

- Gold Open Access
- Publishing charges waived
- Preprints welcome
- Edited by active scientists

Meet the Editors of *ChemistryEurope*

Luisa De Cola
Università degli Studi di Milano Statale, Italy

Ive Hermans
University of Wisconsin-Madison, USA

Ken Tanaka
Tokyo Institute of Technology, Japan

Chemistry–A European Journal
Research Article
doi.org/10.1002/chem.202203384
Chemistry Europe
European Chemical Societies Publishing
www.chemeurj.org

VIP Dinitrogen Activation in the Gas Phase: Spectroscopic Characterization of C–N Coupling in the $V_3C^+ + N_2$ Reaction

Zi-Yu Li[+],[a, c] Francine Horn[+],[b, c] Yao Li,[d, e] Li-Hui Mou,[a] Wieland Schöllkopf,[c] Hui Chen,*[d, e] Sheng-Gui He,*[a, e] and Knut R. Asmis*[b]

Abstract: We report on cluster-mediated C–N bond formation in the gas phase using N_2 as a nitrogen source. The $V_3C^+ + N_2$ reaction is studied by a combination of ion-trap mass spectrometry with infrared photodissociation (IRPD) spectroscopy and complemented by electronic structure calculations. The proposed reaction mechanism is spectroscopically validated by identifying the structures of the reactant and product ions. V_3C^+ exhibits a pyramidal structure of C_1-symmetry. N_2 activation is initiated by adsorption in an end-on fashion at a vanadium site, followed by spontaneous cleavage of the N≡N triple bond and subsequent C–N coupling. The IRPD spectrum of the metal nitride product $[NV_3(C{=}N)]^+$ exhibits characteristic C=N double bond (1530 cm^{-1}) and V–N single bond (770, 541 and 522 cm^{-1}) stretching bands.

Introduction

The controlled formation of carbon-nitrogen (C–N) bonds is of great importance as it opens up opportunities for the incorporation of nitrogen into organic molecules. Such N-containing compounds serve as essential building blocks for natural products, pharmaceuticals, and multifunctional materials.[1] Dinitrogen (N_2) is the most abundant nitrogen source on Earth. Its apolar nature, high ionization potential, negative electron affinity, and strong N≡N triple bond lead to significant challenges in activating dinitrogen and directly assembling C–N bonds.[2] Therefore, the common route to C–N bond formation typically involves nitrogen-containing species derived from ammonia (NH_3). However, there exist several problems in industrial-scale NH_3 production (Haber-Bosch process) such as harsh reaction conditions (350–550 °C and 150–350 atm), high energy consumption (2% of the global annual supply), and substantial global greenhouse gas emission.[3] Therefore, identifying active species that enable C–N bond formation directly from N_2 under mild conditions remains one of the central challenges in heterogenous catalysis.

Gas-phase clusters represent ideal, computationally tractable model systems for highly reactive species. Experiments on these allow for valuable insights into structure-reactivity correlations as well as into fundamental reaction mechanisms that would be hard to obtain from condensed phase studies.[4] The formation of C–N bonds in gas phase reactions has attracted considerable attention in the past decades. Previous studies can be classified into three categories based on the nitrogen sources used, namely, metal nitride species,[5] NH_3,[6] and N_2.[7] The diatomic metal nitride cations ReN^+ and TaN^+ can react with CH_4 to form C–N bonds.[5] Extensive investigations have focused on assembling C–N bonds from the thermal reactions of metal-methyl, methylene, and methylidyne complexes with NH_3.[6] In addition, C–N bond formation has also been reported for reactions of metal carbide anions with N_2.[7] Recently, the coupling of N_2 with CO_2 mediated by NbH_2^- and $AuNbBO^-$,[8] and the coupling of N_2 with CH_4 mediated by $CoTaC_2^-$ have been proposed.[9] Most of these studies rely on a combination of mass spectrometry and quantum chemical calculations to elucidate the nature of electronic structures of the active species and the underlying reaction mechanism. In some cases, collision-induced dissociation or photoelectron spectroscopic experiments have been employed to gain

[a] Dr. Z.-Y. Li,[+] L.-H. Mou, Prof. Dr. S.-G. He
State Key Laboratory for Structural Chemistry of Unstable and Stable Species
Institution of Chemistry
Chinese Academy of Sciences
Beijing 100190 (P. R. China)
E-mail: shengguihe@iccas.ac.cn

[b] F. Horn,[+] Prof. K. R. Asmis
Wilhelm-Ostwald-Institut für Physikalische und Theoretische Chemie
Universität Leipzig
Linnéstrasse 2, 04103 Leipzig (Germany)
E-mail: knut.asmis@uni-leipzig.de

[c] Dr. Z.-Y. Li,[+] F. Horn,[+] Dr. W. Schöllkopf
Fritz-Haber-Institut der Max-Planck-Gesellschaft
Faradayweg 4–6, 14195 Berlin (Germany)

[d] Y. Li, Prof. Dr. H. Chen
CAS Key Laboratory of Photochemistry
Institute of Chemistry
Chinese Academy of Sciences, Beijing 100190 (P. R. China)
E-mail: chenh@iccasac.cn

[e] Y. Li, Prof. Dr. H. Chen, Prof. Dr. S.-G. He
University of Chinese Academy of Sciences
Beijing, 100049 (P. R. China)

[+] These authors contributed equally to this work.

Supporting information for this article is available on the WWW under https://doi.org/10.1002/chem.202203384

structural information, but the unambiguous identification of C–N bond formation in the gas phase using spectroscopic means has not been achieved so far.

Vibrational action spectroscopy has proven particularly useful to characterize the N_2 – metal cluster interaction.[10] Monitoring the red shift of the N_2 stretching frequency (unbound: 2330 cm^{-1}) allows to differentiate between weaker-bound N_2 in an end-on coordination (2330–2100 cm^{-1})[10a–f] and a more strongly interacting side-on coordinated μ_2-N_2 (1500–1400 cm^{-1}).[10g] Cleavage of the N≡N triple bond leads to the formation of metal nitride species, whose presence has been inferred indirectly by spectroscopic identification of an activated N–N intermediate along a computed reaction path that elucidated a stepwise across edge above surface (AEAS) mechanism.[10g] Metal nitride stretching bands are predicted below 800 cm^{-1} and therefore challenging to detect using commercially available tabletop lasers.

Herein, we report on the spectroscopic characterization of the $V_3C^+ + N_2$ reaction. This particular vanadium carbide cation was chosen, because vanadium in the direct vicinity of a carbon atom is useful for dinitrogen fixation. Moreover, it has been indicated that a multinuclear metal center is more effective for dinitrogen activation.[11] We complement the mass spectrometric investigation of the V_3C^+/N_2 reaction couple by vibrational action spectroscopy using the intense and widely wavelength-tunable IR radiation from an IR free electron laser in order to unambiguously identify the structures of the reactant and the product ions. We find that dinitrogen is adsorbed dissociatively, forming predominantly $[NV_3(C{=}N)]^+$, identified by the observation of the IR-active C=N double bond and N V–N–V single bond stretching fundamentals in the fingerprint region of the vibrational action spectrum.

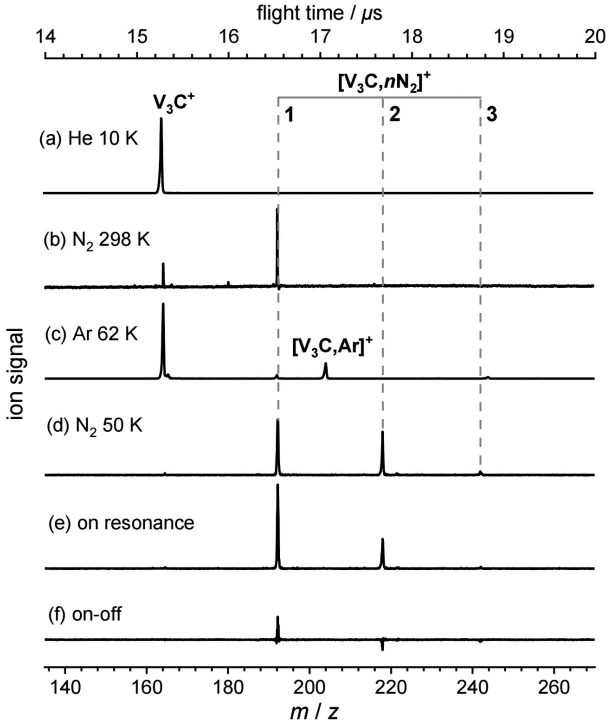

Figure 1. TOF mass spectra for the reactions of mass-selected V_3C^+ with He (a) and 77 mPa N_2 (b) in a linear ion-trap reactor at room temperature for about 1 ms and for the storage of mass-selected V_3C^+ for 200 ms in a cryogenic ring-electrode ion-trap filled with 5% Ar/He at 62 K (c), and 0.004% N_2/He at 50 K (d). Upon resonant excitation of $[V_3C,nN_2]^+$ at wavenumber (υ) of 1520 cm^{-1} (see text below), fragmentation of the weakly bonded adducts ($n>1$) occurs (e). The difference spectrum obtained by subtracting the on-resonance ($\upsilon = 1520$ cm^{-1}) from an off-resonance ($\upsilon = 1470$ cm^{-1}) mass spectrum is shown in (f).

Results and Discussion

V_3C^+ cations are formed by laser ablation and their reactivity toward N_2 is studied in a linear ion-trap reactor.[12] A typical time-of-flight (TOF) mass spectrum for the interaction of mass-selected and subsequently thermalized V_3C^+ cations with N_2 (70 mPa) for ~1 ms at room temperature is shown in Figure 1b. Under these conditions, the adsorption of only a single N_2 molecule is observed [Eq. (1)]:

$$V_3C^+ + N_2 \rightarrow [V_3C,N_2]^+ \quad (1)$$

On the basis of a least-squares fitting procedure (Figure S1), the rate constant (k_1) of the pseudo-first-order reaction of V_3C^+ with N_2 is estimated to be $(8.8 \pm 1.8) \times 10^{-11}$ $cm^3\,molecule^{-1}\,s^{-1}$, corresponding to a reaction efficiency (Φ) of (14.2 ± 2.8)%.[13]

Ion-trap mass spectrometry yields mass-to-charge ratios of the reactant and product ions and hence information on reactivity and stability, but typically no information on geometric and electronic structure. Such information can be obtained from cryogenic ion trap vibrational spectroscopy,[14] which we employ here in combination with messenger-tagging[15] to obtain infrared photodissociation (IRPD) spectra. The IRPD experiments were performed with the Berlin cryogenic ion-trap triple mass spectrometer[16] and using the widely tuneable, intense IR radiation from the Fritz-Haber-Institute Free-Electron-Laser (FHI FEL).[17] As the reactant cation V_3C^+ does not bind He efficiently at 10 K and most likely reacts with H_2 due to the cluster's high reactivity, we chose the more polarizable Ar atom as a messenger for characterization of the reactant ion (Figure 1c). Additional mass spectra are shown in Figures S2 (Supporting Information). For the product ion $[V_3C,N_2]^+$, we exploit an alternative strategy,[18] namely photodissociation of larger $[V_3C,nN_2]^+$ ($n>1$) complexes. Here, we assume that for $n>1$ all additional N_2 molecules are molecularly adsorbed, hence weakly bound and therefore can be used as "innocent" messengers for photodissociation. The corresponding mass spectra are shown in Figure 1d–f. The spectrum in Figure 1e was recorded after irradiating all ions extracted from the ion trap on-resonance (1520 cm^{-1}), and the difference spectrum (Figure 1f) is obtained by subtracting an off-resonance spectrum (1470 cm^{-1}) from this on-resonance spectrum. Using sufficiently attenuated laser-pulse energies, multiple photon absorption is avoided and photodissociation is only observed for the $n>1$ adducts, i.e., peaks associated with $n>1$ are depleted in the on-resonance spectrum (i.e., downward

peaks in Figure 1f), while the $n=1$ peak increases in intensity (i.e., upward peak in Figure 1f).

Figure 2 compares the experimental IRPD spectra of Ar-tagged V_3C^+ at 62 K in the spectral region from 900 to 400 cm^{-1} with IR spectra of bare and Ar-tagged low-energy isomers calculated with density functional theory (DFT) and using the TPSS/TZVP/VPT2 method[19] (see Methods in Supporting Information). The IRPD spectra were measured under different experimental conditions that allow probing photodepletion of V_3C^+ tagged either with one or four Ar-atoms. The IRPD spectrum of $[V_3C,Ar]^+$ (Figure 2a) reveals four bands at ~750 (A), 696 (B), 641 (C) and 618 cm^{-1} (D). In contrast, the relative intensities of these bands are different in the IRPD spectrum of $[V_3C,4Ar]^+$ (Figure 2b) and band D is nearly absent. This confirms, as already noted in previous studies on metal-containing clusters,[20] Ar is not an innocent messenger, but needs to be included in the DFT calculations. Furthermore, a dependence of the IRPD spectrum on the number of (weakly-bound) tags could also indicate the presence of multiple isomers with substantially different sequential Ar binding energies.[20a]

The DFT calculations predict two types of isomers for bare V_3C^+, the energetically lower lying pyramidal structure **R1** with the carbon atom located above the V_3 plane and the higher lying planar structure **R2** (see Figures 2 and S3). For both type of isomers three different spin states (singlet, triplet and quintet) are found rather close in energy with substantially different bond lengths. ^{3}**R1** exhibits C_1 symmetry and is predicted as the most stable isomer, followed by ^{5}**R1** (+8 kJ/mol) and ^{1}**R1** (+37 kJ/mol), both with C_s symmetry. The planar isomer (^{3}**R2**) is found much higher in energy (+69 kJ/mol) and thus is not considered in the following calculations.

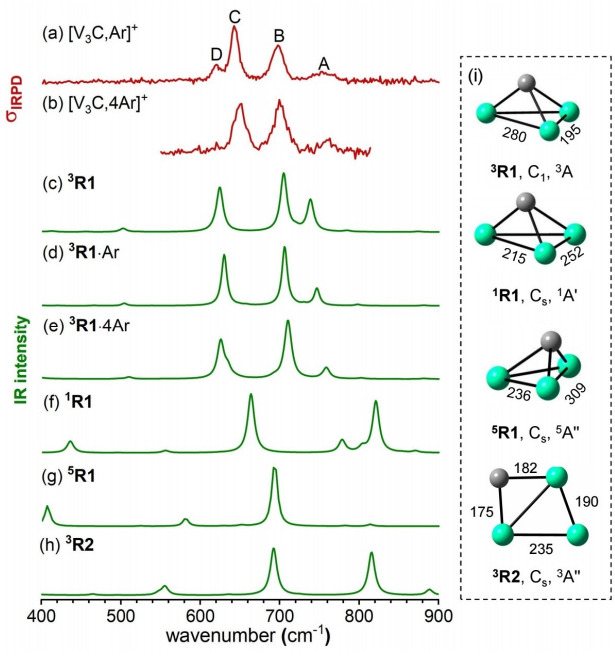

Figure 2. Experimental IRPD spectra (red) of $[V_3C,Ar]^+$ and $[V_3C,4Ar]^+$ at 62 K (a & b) and DFT calculated IR spectra (green) of untagged and Ar-tagged isomers of V_3C^+ (c–h). Geometric structures of the low-lying isomers (i). The symmetries, electronic states, and selected bond lengths in pm are given. The superscript denotes the spin multiplicity. See Table S1 for peak assignments.

To obtain more reliable relative energies of the pyramidal isomers in different spin states, a multiconfigurational method based on density matrix renormalization group strongly contract *n*-electron valence perturbation theory (DMRG-SC-NEVPT2)[21] is employed. The results in the complete basis set (CBS) limit are given in Table 1. The multiconfigurational method yields a different energy ordering with ^{1}**R1** as the global ground state structure. ^{3}**R1** and ^{5}**R1** are +7 kJ/mol and +55 kJ/mol higher in energy, respectively. When the corresponding Ar complexes are considered, the energy difference (relative to ^{1}**R1**·Ar) is reduced to +3 kJ/mol (^{3}**R1**·Ar) and +50 kJ/mol (^{5}**R1**·Ar). Taking the accuracy of ab initio methods for transition metal species into consideration (12 kJ/mol),[22] the formation of ^{5}**R1** can be ruled out. However, which of the two lower spin isomers, ^{1}**R1** or ^{3}**R1**, is present in the experiment cannot be conclusively determined based on the results in Table 1.

Based on the comparison of the experimental to the predicted IR spectra, the spectrum of ^{3}**R1** (Figure 2c) is the best match. In contrast to the spectra of ^{1}**R1** (Figure 2f), ^{5}**R1** (Figure 2g), and ^{3}**R2** (Figure 2h), the spectrum of ^{3}**R1** reproduces the three highest energy bands (A–C in Figures 2a and 2b) reasonably. Bands B and C then correspond to the fundamentals of C–V_3 stretching and V–C–V bending modes, respectively. Band A is attributed to an overtone of V–V–C bending mode. None of the predicted spectra reproduce band D and therefore it is unlikely that it is due to the presence of a second isomer. Interestingly, band D is absent from the IRPD spectrum of $[V_3C,4Ar]^+$ (Figure 2b), suggesting that the additional Ar tags may lead to a blue shift of this feature into the spectral region of band C. The predicted IR spectra of ^{3}**R1**·Ar and ^{3}**R1**·4Ar show a satisfactory agreement with the corresponding experimental spectra and provide evidence that band D probably can be attributed to a combination band involving excitation of V–V stretching and V–V–C bending modes. This combination band is predicted 5 cm^{-1} below the V–C–V bending modes (band C) for ^{3}**R1**·Ar, while for ^{3}**R1**·4Ar the energetic order is reversed and it is predicted 9 cm^{-1} above the V–C–V bending modes (Table S2). This does not only rationalize the absence of band D in IRPD spectrum of ^{3}**R1**·4Ar, but also the appearance of a shoulder at 659 cm^{-1}, i.e. on the higher energy side of band C in Figure 2b.

Table 1. Relative electronic energies (ΔE), zero-point-energy-corrected relative energies (ΔE_0) and Ar-binding energies (BE_0) of low-energy V_3C^+ Isomers calculated using DFT[a] and multiconfigurational method.[b] All energies are given in kJ/mol.

Isomer	ΔE_{DFT}	$\Delta E_{0,DFT}$[d]	ΔE_{NEVPT2}[c]	$\Delta E_{0,NEVPT2/DFT}$[c,d]	$BE_{0,DFT}$
^{1}**R1**	34	37	0	0	12
^{3}**R1**	0	0	9	7	16
^{5}**R1**	9	8	58	55	15
^{3}**R2**	66	69	–	–	–

[a] TPSS/TZVP. [b] NEVPT2/CBS. [c] At the DFT minimum-energy geometry. [d] ZPE-correction determined from harmonic DFT vibrational frequencies.

After identifying the structure of the reactant ion, we turn our focus to the product of the $V_3C^+ + N_2$ reaction. Figure 3a shows the experimental IRPD spectrum of $[V_3C,2\,N_2]^+$. It exhibits four features in the spectral region from 1700 to 400 cm^{-1}, an intense band at 1524 cm^{-1} (labeled E in Figure 3a) as well as three less intense features at 770 (F), 541 (G), and 520 cm^{-1} (H). Genetic algorithm based global optimization is employed to search the global minimum-energy structure. The results and the corresponding IR spectra of these isomers are shown in Figures 3 and S5.

Two energetically competitive isomers, **P1** and **P2**, are predicted by DFT. The metal nitride structure **P1** (see Figure 3), formed by dissociative adsorption of dinitrogen, is predicted as the global ground state. Its structure can be written as $[NV_3(C{\equiv}N)]^+$. It contains a 3-fold coordinated nitrogen atom (μ_3-N) and a C≡N unit binding to the V_3 core in the end-on/side-on/side-on configuration (μ_3-η^1:η^2:η^2). **P2** has two 2-fold coordinated N atoms (μ_2-N) and one 3-fold coordinated C atom (μ_3-C) and its structure can be written as $[(\mu_2\text{-N})_2V_3(\mu_3\text{-C})]^+$. DFT calculations predict ^{3}**P1** as the energetically lowest lying isomer of $[V_3C,N_2]^+$, followed by ^{3}**P2** (+1 kJ/mol), ^{1}**P1** (+18 kJ/mol) and ^{1}**P2** (+41 kJ/mol), see Table S3. Furthermore, the RCCSD(T) method (partially spin-adapted open-shell coupled cluster method with single, double, and perturbative triple excitations)[23] is adopted to calculate the single point energies of the DFT-optimized structures to obtain more reliable relative energy because no obvious multireference characters are observed for product isomers (see Supporting Information). A different energy ordering is given by RCCSD(T) calculations with the singlet state ^{1}**P1** as the global ground state. The other isomers are found much higher in energy (+20 kJ/mol for ^{3}**P1**, +45 kJ/mol for ^{1}**P2** and +74 kJ/mol for ^{3}**P2**) and are not considered any further.

The predicted IR spectrum of ^{1}**P1** (Figure 3c) is in good agreement with the experimental IRPD spectrum with respect to band positions and relative intensities. Consideration of the second, weakly bound N_2 molecule in the calculations (Figure 3b, see Table S1 for band assignments) improves this agreement. The four observed characteristic bands E–H prove to be particularly diagnostic for the formation of the C=N bond (and hence rupture of the N≡N bond). Bands E, F, and H are assigned to excitation of the C=N stretching as well as the symmetric and the antisymmetric V–N–V stretching fundamentals, respectively. Band G is attributed to the V–NC stretching mode. The predicted IR spectra of the higher energy isomers ^{3}**P1** and ^{1}**P2** show worse agreement with the experimental IRPD spectrum and we therefore conclude that dinitrogen is adsorbed dissociatively forming ^{1}**P1**.

To obtain mechanistic insights into the $V_3C^+ + N_2$ reaction, the reaction mechanism was interrogated by electronic structure calculations. The RCCSD(T)/CBS potential-energy surface (PES) of the most favorable reaction pathway as well as the relevant structures are shown in Figure 4. We find that the reaction can be initiated either from ^{1}**R1** or ^{3}**R1** (Figure S8). However, it proceeds barrierless (with respect to the energy of entrance channel) only on the singlet PES and we therefore consider only this pathway in the following discussion.

As shown in Figure 4, the highly exothermic reaction commences with N_2 coordinated to one V atom in an end-on fashion to form intermediate ^{1}**1** (−54 kJ/mol), in which the N≡N triple bond is only slightly activated (110 pm in free N_2 vs. 115 pm in ^{1}**1**). The second V atom then interacts with the terminal N atom (labeled as N2) and intermediate ^{1}**2** (−117 kJ/mol) is formed via transition structure ^{1}**1/2** (−33 kJ/mol). In ^{1}**2** N_2 is anchored by two V atoms in the known side-on/end-on

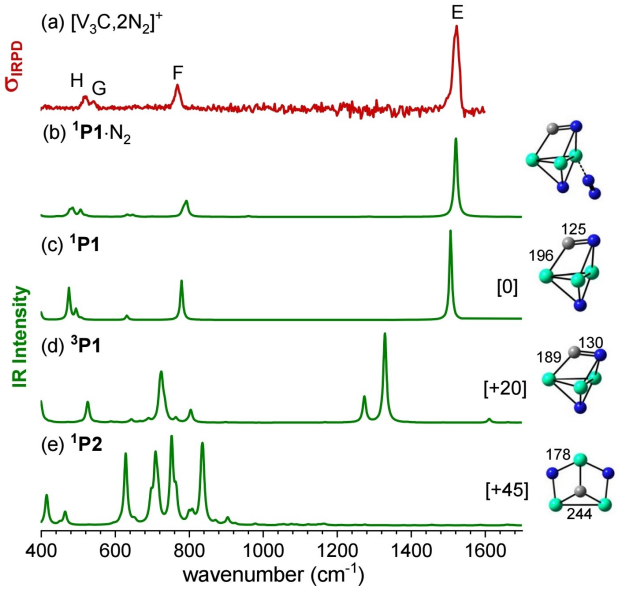

Figure 3. Experimental IRPD spectrum (red) of $[V_3C,2\,N_2]^+$ at 50 K (a), and IR spectra calculated with DFT of ^{1}**P1**·N_2 (b), ^{1}**P1** (c), ^{3}**P1** (d), and ^{1}**P2** (e). The zero-point corrected energies (ΔE_0) at the RCCSD(T) level of theory with respect to ^{1}**P1** are given in kJ/mol. Some bond lengths are given in pm. See Table S1 for peak assignments. The superscript denotes the spin multiplicity.

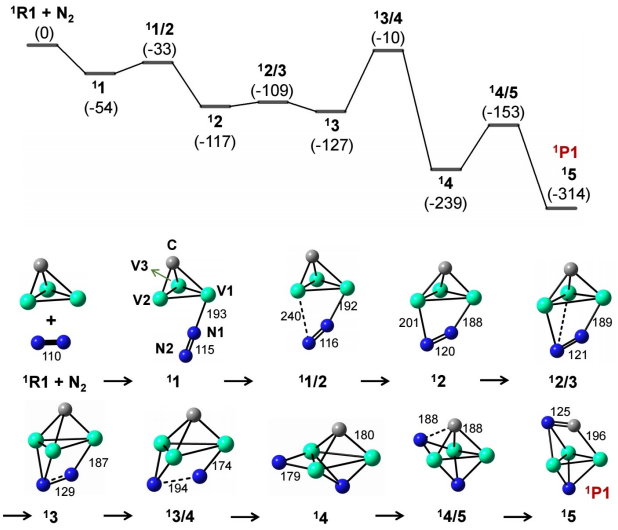

Figure 4. RCCSD(T) energy profile for the reaction of V_3C^+ with N_2. The zero-point corrected relative energies (ΔE_0) with respect to the separate reactants ^{1}**R1** + N_2 are given in kJ/mol. Some bond lengths are listed in pm. The superscript denotes the spin multiplicity.

mode and the N_2 bond distance increases to 120 pm. Through a structural rearrangement, the N_2 unit is bound to three metal atoms in the end-on/side-on/side-on configuration to form a more stable intermediate ^{1}**3** (−127 kJ/mol) where the N–N bond is further elongated to 129 pm. Subsequently, by overcoming the transition structure ^{1}**3/4** (−10 kJ/mol), the complete rupture of the N–N bond occurs, readily forming intermediate ^{1}**4** (−239 kJ/mol) containing two bridging N atoms. Note, that the computed pathway up to ^{1}**4** shown in Figure 4 corresponds to the AEAS mechanism predicted in the case of $Ta_4^+ + N_2$.[10g] C–N coupling then proceeds via transition structure ^{1}**4/5** (−153 kJ/mol), finally leading to the formation of the product ion ^{1}**P**$_1$ (−314 kJ/mol). The overall reaction is exothermic by more than 300 kJ/mol. The possibility of subsequent dissociative adsorption of a second N_2 molecule was also considered (Figure S9), but is unlikely, as it involves a substantial positive energy barrier (+45 kJ/mol).

If the reaction involves the formation of ^{1}**P1** from ^{3}**R1**, as the previous analysis of the experimental data suggest, spin crossover from the high spin state to low spin state needs to take place along the reaction pathway.[24] A likely spin crossing point between the triplet and singlet PESs is along the process of ^{3}**1/2**→^{1}**2** (Figure S10). The relative energy of the crossing point is much lower than the separate reactants, suggesting that the spin crossover from triplet to singlet PES is feasible, which supports the observation of product ions in singlet spin-state (^{1}**P1**) in the IRPD experiment.

Conclusions

In summary, the gas-phase reaction of V_3C^+ with N_2 has been studied using ion-trap mass spectrometry combined with IRPD spectroscopy and DFT calculations. The structures of both reactant and product ions have been spectroscopically characterized. The IR signatures of the adsorption products consisting of the C≡N stretching and V–N–V stretching modes spectroscopically confirm the cleavage of the N≡N triple bond and the subsequent C–N coupling. The computed reaction path follows a mechanism that corresponds to the previously suggested AEAS mechanism, but proceeds further towards C–N coupling.

Experimental Section

Cluster reactivity: The reactivity of vanadium carbide cluster cations ($V_xC_y^+$) was investigated on a time-of-flight (TOF) mass spectrometer coupled with a laser ablation source, a quadrupole mass filter, and a linear ion trap.[12] The vanadium carbide cluster cations were generated by laser ablation of a vanadium disk target in the presence of 0.5% CH_4 seeded in a He carrier gas with a backing pressure of 6 standard atmospheres. The clusters of interest were mass-selected using a quadrupole mass-filter and entered into a linear ion-trap reactor, where they were confined and cooled by multiple collisions with a pulse of He gas for about 1.0 ms and then interacted with a pulse of N_2 for about 1.0 ms. The temperature of the cooling gas (He), the reactant gas (N_2), and the ion trap was around 298 K.[25] The reactant and product cluster ions then were ejected from the ion trap and focused into the extraction region of a reflectron TOF mass spectrometer to obtain mass (to charge ratio) and abundance information.

Structural characterization: The infrared photodissociation (IRPD) experiments were performed employing a cryogenic ion trap tandem mass spectrometer[16] using the widely tunable, intense IR radiation from the Fritz-Haber-Institute Free-Electron-Laser (FHI FEL).[17] In brief, $V_xC_y^+$ ions were generated in a pulsed laser vaporization source by focusing a frequency-doubled Nd:YAG laser (50 Hz, 10–15 mJ) onto a rotating vanadium metal rod. The resulting plasma was quenched with a gas pulse of 0.5% CH_4 seeded in He. Cluster ions were formed during expansion through a clustering channel downstream from the rod and passed through a skimmer. The beam of ions was then collimated and thermalized close to room temperature in a He-gas filled radio frequency (RF) ion guide, mass-selected using a quadrupole mass-filter, and focused into a cryogenically cooled RF ring-electron ion-trap. The trap was continuously filled with a gas mix of 5% Ar in He gas or a reactant gas/buffer gas mix of 0.004% N_2 in He gas at an ion-trap temperature of 62 K and 50 K, respectively. Many collisions of the trapped ions with the gas particles provided gentle cooling of the internal degrees of freedom close to the ambient temperature. Under these conditions, the Ar-tagged V_3C^+ or the N_2-tagged $[V_3C,N_2]^+$ were formed. For the IRPD experiments of the $[V_3C,n\mathrm{Ar}]^+$ complex we used the Ar atoms as a messenger tag at 62 K. By varying the delay time of the electric field pulse that extracts ions from the trap and accelerates them towards the TOF mass spectrometer, we could irradiate $[V_3C,n\mathrm{Ar}]^+$ ions with $n \leq 1$ and $n \leq 4$ with the radiation from the free electron laser to obtain the experimental spectra of $[V_3C,\mathrm{Ar}]^+$ and $[V_3C,4\mathrm{Ar}]^+$, respectively. For the IRPD experiments of the $[V_3C,2\ N_2]^+$ complex, the second N_2 molecule served as a messenger tag at 50 K. All ions were extracted from the ion trap at 5 Hz and focused both temporally and spatially into the center of the extraction region of an orthogonally mounted reflection TOF tandem photofragmentation mass-spectrometer. Here, the ions were irradiated with a counter-propagating IR laser pulse produced by the FHI FEL (400–1600 cm^{-1}, bandwidth: ~0.5% fwhm, pulse energy: 3.5~8 mJ). All parent and photofragment ions were then accelerated towards a microchannel plate detector and monitored simultaneously. The IRPD spectrum was obtained by recording the photofragmentation yield as a function of the laser wavelength. The scans were recorded by averaging 100 TOF mass spectra per wavelength step (3 cm^{-1}) and scanning the wavelength of the laser. Typically, at least three scans were summed. The photodissociation cross section σ_{IRPD} was determined as described previously.[14]

Acknowledgements

This work was financially supported by the K. C. Wong Education Foundation, the National Natural Science Foundation of China (Nos. 21833011, 21973101, and 22173111), the Youth Innovation Promotion Association CAS (No. 2020034). KRA acknowledges financial support by the Deutsche Forschungsgemeinschaft (DFG, German Research Foundation) within project 430942176 "Mixed Metal Oxide Clusters: Model Systems for Catalytically Active Materials" (Asmis/Sauer). We greatly acknowledge the skillful assistance of Sandy Gewinner during the FHI FEL beam time sessions. Open Access funding enabled and organized by Projekt DEAL.

Conflict of Interest

The authors declare no conflict of interest.

Data Availability Statement

The data that support the findings of this study are available from the corresponding author upon reasonable request.

Keywords: atomic cluster · C–N coupling · infrared photodissociation · nitrogen activation · reaction mechanism

[1] a) Z.-J. Lv, J. Wei, W.-X. Zhang, P. Chen, D. Deng, Z.-J. Shi, Z. Xi, *Natl. Sci. Rev.* **2020**, *7*, 1564–1583; b) C. Chen, X. Zhu, X. Wen, Y. Zhou, L. Zhou, H. Li, L. Tao, Q. Li, S. Du, T. Liu, D. Yan, C. Xie, Y. Zou, Y. Wang, R. Chen, J. Huo, Y. Li, J. Cheng, H. Su, X. Zhao, W. Cheng, Q. Liu, H. Lin, J. Luo, J. Chen, M. Dong, K. Cheng, C. Li, S. Wang, *Nat. Chem.* **2020**, *12*, 717–724; c) S. Kim, F. Loose, P. J. Chirik, *Chem. Rev.* **2020**, *120*, 5637–5681.

[2] C.-G. Zhan, J. A. Nichols, D. A. Dixon, *J. Phys. Chem. A* **2003**, *107*, 4184–4195.

[3] a) H. Li, C. Mao, H. Shang, Z. Yang, Z. Ai, L. Zhang, *Nanoscale* **2018**, *10*, 15429–15435; b) A. J. Medford, M. C. Hatzell, *ACS Catal.* **2017**, *7*, 2624–2643; c) H.-P. Jia, E. A. Quadrelli, *Chem. Soc. Rev.* **2014**, *43*, 547–564; d) D. Singh, W. R. Buratto, J. F. Torres, L. J. Murray, *Chem. Rev.* **2020**, *120*, 5517–5581.

[4] a) C. Geng, J. Li, T. Weiske, H. Schwarz, *Proc. Natl. Acad. Sci. USA* **2018**, *115*, 11680–11687; b) S. M. Lang, T. M. Bernhardt, *Phys. Chem. Chem. Phys.* **2012**, *14*, 9255–9269; c) H. Schwarz, K. R. Asmis, *Chem. Eur. J.* **2019**, *25*, 2112–2126; d) G. Liu, I. R. Ariyarathna, S. M. Ciborowski, Z. Zhu, E. Miliordos, K. H. Bowen, *J. Am. Chem. Soc.* **2020**, *142*, 21556–21561; e) N. Levin, J. Lengyel, J. F. Eckhard, M. Tschurl, U. Heiz, *J. Am. Chem. Soc.* **2020**, *142*, 5862–5869; f) J. Yamagishi, K. Miyajima, S. Kudoh, F. Mafuné, *J. Phys. Chem. Lett.* **2017**, *8*, 2143–2147; g) F. Mafuné, Y. Tawaraya, S. Kudoh, *J. Phys. Chem. A* **2016**, *120*, 4089–4095; h) R. A. J. O'Hair, G. N. Khairallah, *J. Cluster Sci.* **2004**, *15*, 331–363.

[5] a) S. D. Zhou, J. L. Li, M. Schlangen, H. Schwarz, *Angew. Chem. Int. Ed.* **2016**, *55*, 11678–11681; *Angew. Chem.* **2016**, *128*, 11851–11855; b) S. Zhou, J. Li, M. Schlangen, H. Schwarz, *Angew. Chem. Int. Ed.* **2016**, *55*, 14863–14866; *Angew. Chem.* **2016**, *128*, 15085–15089.

[6] a) R. Kretschmer, M. Schlangen, H. Schwarz, *Dalton Trans.* **2013**, *42*, 4153–4162; b) R. Kretschmer, M. Schlangen, M. Kaupp, H. Schwarz, *Organometallics* **2012**, *31*, 3816–3824; c) B. Butschke, H. Schwarz, *Chem. Eur. J.* **2011**, *17*, 11761–11772; d) K. Koszinowski, D. Schröder, H. Schwarz, *Organometallics* **2004**, *23*, 1132–1139.

[7] a) Z.-Y. Li, Y. Li, L.-H. Mou, J.-J. Chen, Q.-Y. Liu, S.-G. He, H. Chen, *J. Am. Chem. Soc.* **2020**, *142*, 10747–10754; b) Z.-Y. Li, L.-H. Mou, G.-P. Wei, Y. Ren, M.-Q. Zhang, Q.-Y. Liu, S.-G. He, *Inorg. Chem.* **2019**, *58*, 4701–4705; c) L.-H. Mou, Y. Li, Z.-Y. Li, Q.-Y. Liu, Y. Ren, H. Chen, S.-G. He, *J. Phys. Chem. Lett.* **2020**, 9990–9994; d) L.-H. Mou, Y. Li, Z.-Y. Li, Q.-Y. Liu, H. Chen, S.-G. He, *J. Am. Chem. Soc.* **2021**, *143*, 19224–19231.

[8] a) M. Wang, L.-Y. Chu, Z.-Y. Li, A. M. Messinis, Y.-Q. Ding, L. Hu, J.-B. Ma, *J. Phys. Chem. Lett.* **2021**, *12*, 3490–3496; b) Y. Li, Y.-Q. Ding, S. Zhou, J.-B. Ma, *J. Phys. Chem. Lett.* **2022**, *13*, 4058–4063; c) L.-Y. Chu, Y.-Q. Ding, M. Wang, J.-B. Ma, *Phys. Chem. Chem. Phys.* **2022**, *24*, 14333–14338; d) Z.-Y. Chen, M. Wang, J.-B. Ma, *Chem. Eur. J.* **2022**, *28*, e202201170.

[9] L.-H. Mou, Y. Li, G.-P. Wei, Z.-Y. Li, Q.-Y. Liu, H. Chen, S.-G. He, *Chem. Sci.* **2022**, *13*, 9366–9372.

[10] a) R. A. de Paola, F. M. Hoffmann, D. Heskett, E. W. Plummer, *Phys. Rev. B* **1987**, *35*, 4236–4249; b) C. Kerpal, D. J. Harding, J. T. Lyon, G. Meijer, A. Fielicke, *J. Phys. Chem. C* **2013**, *117*, 12153–12158; c) A. Straßner, C. Wiehn, M. P. Klein, D. V. Fries, S. Dillinger, J. Mohrbach, M. H. Prosenc, P. B. Armentrout, G. Niedner-Schatteburg, *J. Chem. Phys.* **2021**, *155*, 244305; d) M. P. Klein, A. A. Ehrhard, J. Mohrbach, S. Dillinger, G. Niedner-Schatteburg, *Top. Catal.* **2018**, *61*, 106–118; e) S. Dillinger, J. Mohrbach, G. Niedner-Schatteburg, *J. Chem. Phys.* **2017**, *147*, 184305; f) M. P. Klein, A. A. Ehrhard, M. E. Huber, A. Straßner, D. V. Fries, S. Dillinger, J. Mohrbach, G. Niedner-Schatteburg, *J. Chem. Phys.* **2022**, *156*, 014302; g) D. V. Fries, M. P. Klein, A. Steiner, M. H. Prosenc, G. Niedner-Schatteburg, *Phys. Chem. Chem. Phys.* **2021**, *23*, 11345–11354.

[11] a) Y. Kokubo, C. Yamamoto, K. Tsuzuki, T. Nagai, A. Katayama, T. Ohta, T. Ogura, Y. Wasada-Tsutsui, Y. Kajita, S. Kugimiya, H. Masuda, *Inorg. Chem.* **2018**, *57*, 11884–11894; b) Y. Tanabe, Y. Nishibayashi, *Coord. Chem. Rev.* **2019**, *381*, 135–150; c) M. Falcone, L. Chatelain, R. Scopelliti, I. Živković, M. Mazzanti, *Nature* **2017**, *547*, 332.

[12] Z. Yuan, Z.-Y. Li, Z.-X. Zhou, Q.-Y. Liu, Y.-X. Zhao, S.-G. He, *J. Phys. Chem. C* **2014**, *118*, 14967–14976.

[13] a) G. Gioumousis, D. P. Stevenson, *J. Chem. Phys.* **1958**, *29*, 294–299; b) G. Kummerlöwe, M. K. Beyer, *Int. J. Mass Spectrom.* **2005**, *244*, 84–90.

[14] a) N. Heine, K. R. Asmis, *Int. Rev. Phys. Chem.* **2015**, *34*, 1–34; b) N. Heine, K. R. Asmis, *Int. Rev. Phys. Chem.* **2016**, *35*, 507–507.

[15] a) M. Brümmer, C. Kaposta, G. Santambrogio, K. R. Asmis, *J. Chem. Phys.* **2003**, *119*, 12700–12703; b) K. R. Asmis, *Phys. Chem. Chem. Phys.* **2012**, *14*, 9270–9281.

[16] a) D. J. Goebbert, T. Wende, R. Bergmann, G. Meijer, K. R. Asmis, *J. Phys. Chem. A* **2009**, *113*, 5874–5880; b) D. J. Goebbert, G. Meijer, K. R. Asmis, *AIP Conf. Proc.* **2009**, *1104*, 22–29.

[17] W. Schöllkopf, S. Gewinner, H. Junkes, A. Paarmann, G. von Helden, H. Bluem, A. M. Todd, *The new IR and THz FEL facility at the Fritz Haber Institute in Berlin, Vol. 9512*, SPIE, **2015**.

[18] a) Y.-K. Li, S. Debnath, M. Schlangen, W. Schöllkopf, K. R. Asmis, H. Schwarz, *Angew. Chem. Int. Ed.* **2019**, *58*, 18868–18872; *Angew. Chem.* **2019**, *131*, 19044–19048; b) Y.-K. Li, F. Müller, W. Schöllkopf, K. R. Asmis, J. Sauer, *Angew. Chem. Int. Ed.* **2022**, e202202297.

[19] a) J. Tao, J. P. Perdew, V. N. Staroverov, G. E. Scuseria, *Phys. Rev. Lett.* **2003**, *91*, 146401; b) A. Schafer, C. Huber, R. Ahlrichs, *J. Chem. Phys.* **1994**, *100*, 5829–5835; c) J. Bloino, V. Barone, *J. Chem. Phys.* **2012**, *136*, 124108.

[20] a) K. R. Asmis, T. Wende, M. Brümmer, O. Gause, G. Santambrogio, E. C. Stanca-Kaposta, J. Döbler, A. Niedziela, J. Sauer, *Phys. Chem. Chem. Phys.* **2012**, *14*, 9377–9388; b) K. R. Asmis, *Phys. Chem. Chem. Phys.* **2012**, *14*, 9270–9281.

[21] a) S. Guo, M. A. Waston, W. F. Hu, Q. M. Sun, G. K.-L. Chan, *J. Chem. Theory Comput.* **2016**, *12*, 1583–1591; b) A. Y. Sokolva, S. Guo, E. Ronca, G. K.-L. Chan, *J. Chem. Phys.* **2017**, *146*, 244102–244106.

[22] M. Feldt, Q. M. Phung, *Eur. J. Inorg. Chem.* **2022**, e202200014.

[23] a) J. D. Watts, J. Gauss, R. J. Bartlett, *J. Chem. Phys.* **1993**, *98*, 8718–8733; b) P. J. Knowles, C. Hampel, H. J. Werner, *J. Chem. Phys.* **1993**, *99*, 5219–5227.

[24] a) D. Schroder, S. Shaik, H. Schwarz, *Acc. Chem. Res.* **2000**, *33*, 139–145; b) J. N. Harvey, M. Aschi, H. Schwarz, W. Koch, *Theor. Chem. Acc.* **1998**, *99*, 95–99.

[25] Y.-X. Zhao, Z.-Y. Li, Z. Yuan, X.-N. Li, S.-G. He, *Angew. Chem. Int. Ed.* **2014**, *53*, 9482–9486; *Angew. Chem.* **2014**, *126*, 9636–9640.

Manuscript received: November 1, 2022
Accepted manuscript online: December 13, 2022
Version of record online: February 6, 2023